Investigation of the Effects of Needle Designs on the Root Canal Irrigation Using Computational Fluid Dynamics

Farklı İğne Tasarımlarının Diş Kanalı İrrigasyonu Üzerindeki Etkilerinin Hesaplamalı Akışkanlar Dinamiği ile İncelenmesi

Alperen Yıldızeli [1*] , **Selin Bulgu** [2] , **Sertaç Çadırcı** [1] , **Sema Yıldırım** [2]

[1] Department of Mechanical Engineering, İstanbul Technical University, İstanbul, Turkey
[2] Department of Endodontics, İstanbul University, Faculty of Dentistry, İstanbul, Turkey
Sorumlu Yazar / Corresponding Author *: yildizeli@itu.edu.tr

Abstract

This study aims to investigate the effects of irrigation needles geometries on the flow inside the root canal and compare their irrigation performances based on Computational Fluid Dynamics (CFD) analyzes. CFD simulations of three commonly used close-ended irrigation needles were performed for various inlet Reynolds numbers and working lengths. Their irrigation performances were evaluated based on apical pressure and wall shear stress. The flow was assumed to be incompressible, turbulent and steady at all inlet Reynolds numbers. The closed-ended needles showed similar limited irrigant penetration toward the apex. Among all configurations, the Model C outperforms others as it provides the highest wall shear stress around the needle tip and the lowest apical pressures in the apical foramen, which reduces the risk of apical extrusion. The needle tip designs influence important parameters for the effectiveness and safety of the irrigation process.
Keywords: Computational Fluid Dynamics (CFD), Endodontics, Irrigation, Needle Tip Design

Özet

Bu çalışma, bir dişin kök kanalının irrigasyonunda kullanılan iğnelerinin geometrilerinin kök kanalı içindeki akış üzerine etkilerini araştırmayı ve bunların irrigasyon performanslarını "Hesaplamalı Akışkanlar Dinamiği (HAD)" analizlerine dayanarak karşılaştırmayı amaçlamaktadır. Çeşitli giriş Reynolds sayıları ve çalışma uzunlukları için yaygın olarak kullanılan üç adet yandan perfore irrigasyon iğnesinin HAD simülasyonları yapıldı. Bunların irrigasyon performansları apikal bölgedeki ortalama basınç ve kanal boyunca ortalama duvar kayma gerilmesine dayalı olarak değerlendirildi. İncelenen tüm giriş Reynolds sayılarında akışın sıkıştırılamaz, türbülanslı ve daimi olduğu varsayıldı. İncelenen yandan perfore iğnelerin irrigasyon performansı apekse doğru ilerledikçe benzer şekilde doyuma ulaşmaktadır. Tüm konfigürasyonlar arasında Model C, iğne ucu çevresinde en yüksek duvar kayma gerilimini ve apikal foramende en düşük apikal basınçları sağlayarak apikal ekstrüzyon riskini azalttığı için diğerlerinden daha iyi performans gösterdi. İğne ucu tasarımları, irrigasyonun verilmiliği ve güvenliği için önemli parametreleri etkilemektedir.
Anahtar Kelimeler: Hesaplamalı Akışkanlar Dinamiği, Endodonti, İrigasyon, İğne Ucu Tasarımı

1. Introduction

Root canal treatment aims to treat endodontic infections and to provide periapical healing [1]. The main objective of root canal treatment is to achieve disinfected and clean root canal before the filling to avoid bacterial re-colonization [2]. One of the biological aims of the root canal preparation is to remove debris from the root canal system which has a complex anatomy and numerous irregularities such as lateral canals, deltas, and isthmuses ([3],[4]). Studies showed with only mechanical instrumentation about half of the root canal surface area remained uninstrumented [5], [6], [7] [8]. Therefore, irrigation is essential to remove debris and to obtain disinfected root canal system, although there are new methods for root canal irrigation, such as sonic or ultrasonic activation, the conventional root canal irrigation method still has common use among dentists for root canal treatment [9]. Effectiveness and the safety of the root canal irrigation depends on several factors and various methods have been proposed to test these parameters in the last decade ([10], [11], [12], [13], [14] and [15]), however these methods provided insufficient insight into the irrigation process [16]. Computational Fluid Dynamics (CFD) is finite-volume based numerical solution technique for fluid dynamics problems [17]. CFD is a powerful method to evaluate flow characteristics by means of streamlines, velocity distributions, shear stresses and pressure on the root canal wall, that are difficult to measure in vivo due to the complex anatomy of the root canal [16]. CFD can be considered as a promising tool to investigate the effect of needle tip design on root canal irrigation and potential irrigant extrusion risks, as in many engineering problems. In this study, the effects of irrigation needles with various tip designs on the efficiency of irrigation in a maxillary central incisor root canal have been investigated by parametric CFD analyzes.

2. Materials and Methods

The use of an extracted tooth was approved by Istanbul University Faculty of Dentistry Clinical Research Ethics Committee (2019/31). A maxillary central incisor tooth was obtained, and standard access cavity was prepared. A stainless-steel K-file of size 15 (Dentsply Maillefer, Bellaigues, Switzerland) was inserted to the root canal until it was visible at the major apical foramen. Working length (H) was set at 0.5 mm

shorter than the distance from the major apical foramen and a glide path was prepared with the same file before using rotary files. The root canal was prepared with VDWRotate rotary Ni-Ti files (VDW, Munich, Germany) from size 15/.04 taper up to size 45/.04 taper, between every instrument the root canal was rinsed with 2% sodium hypochlorite (NaOCl) (Chloraxid, Cerkamed, Stalowa Wola, Poland). The tooth was scanned with the SkyScan 1275 (Bruker, Kontich, Belgium) micro-CT device which operates at 80kV and 125 μA, using 8 μm voxel size and 49 ms exposure time. Then scans were reconstructed to obtain three-dimensional image of the root canal as shown in Figure 1.

Figure 1. Three-dimensional image of the root canal with the inserted needle from different views: (a) front, (b) side, (c) CAD model

Three closed-ended side-vented root canal irrigation needles were used in the current study. The dimensions of the needles were obtained through x40 magnification images taken under a stereoscopic microscope. (Olympus SZ61, Olympus KeyMed Comp., Tokyo, Japan). Using these dimensions, three-dimensional CAD models were created using the

software Blender 2.82 (Blender Foundation, Amsterdam, Netherlands), as shown in Figure 2.
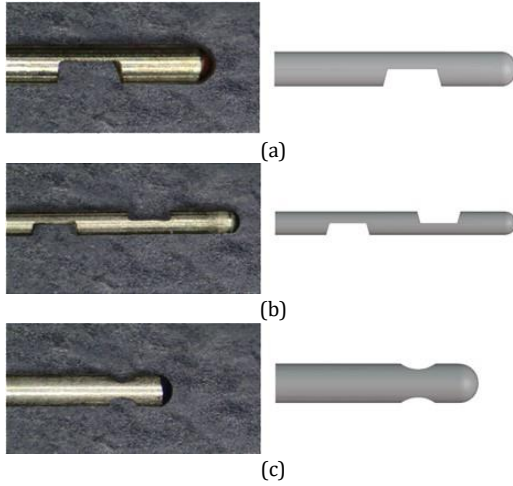

(a)

(b)

(c)

Figure 2. Commercially available closed-ended side-vented irrigation needles and their CAD models: a) closed-ended side-vented irrigation needle (CERKAMED Endo-Top, PPH CERKAMED, Stalowa Wola, Poland), b) closed-ended double-side-vented irrigation needle (Ultradent Navitip, Ultradent Products Inc., South Jordan, UT, USA), and c) closed-ended double-side-vented irrigation needle (GNC Endo Irrigation, Tribest Dental Products, Jiangsu, China).

All needle sizes were standardized to 30-gauge to compare the effect of different designs of needle tips in the study without including the effect of the needle sizes (external diameter of D_{ext}=320 mm, internal diameter of D_{int}=196 mm, and length of L=31 mm). The needles were positioned in the root canal at the distances of H=0.5mm, 1mm, 1.5mm, 2mm and 3mm away from the major apical foramen. The root canal and the needles were assumed to be filled with aqueous solution of NaOCl 2% as the irrigant fluid which is an incompressible Newtonian fluid with a density ρ = 1040kg/m³ and viscosity μ = 0.99×10^{-3}Pa.s [18]. The fluid was allowed to flow from the distal end of the needle and out from the orifice of the root canal. Inlet Reynolds number of the flow ranged from 500 to 1500.

In this section, the irrigation needle to be used for endodontic treatments is introduced by showing the computational domain and imposed boundary conditions. The CFD approach, turbulence model, and necessary mesh convergence tests are explained in detail. To construct an adequate numerical setup; boundary conditions, model properties, convergence criteria and discretization schemes have been determined in accordance with other numerical studies available in the literature. All CFD simulations were performed for steady-state and isothermal conditions using an irrigation needle with a hydraulic diameter of 0.196 mm. Since NaOCl was considered as the irrigation fluid, the flow is incompressible and single-phase. The commercial CFD code ANSYS Fluent 17.2 (Fluent Inc., Lebanon, NH, USA), a finite-volume-based flow solver, was used to carry out the simulations of irrigant flow during root canal irrigation. The flow fields calculated for all needle models were compared in terms of the flow pattern, velocity magnitude, wall shear stress and apical pressure. The continuity equation in Eq. (1), RANS equations in Eq. (2) together with transport equations for k-ω SST turbulence model in Eqs. (3-4) were solved numerically until their convergence criteria were met. Pressure-velocity coupling was managed by using COUPLED algorithm to satisfy numerical convergence. The convergence criteria for continuity, momentum, and turbulence were determined as 10^{-3}, 10^{-4} and 10^{-4}, respectively. Readers may refer to ([19], [20]) to get more information about the k – ω SST turbulence model.

$$\frac{\partial \rho}{\partial t} + \frac{\partial (\rho u_i)}{\partial x_i} = 0 \qquad (1)$$

$$\frac{\partial (\rho u_i)}{\partial t} + \frac{\partial (\rho u_i u_j)}{\partial x_j} = -\frac{\partial p}{\partial x_i} + \frac{\partial}{\partial x_j}\left[\mu\left(\frac{\partial u_i}{\partial x_j} + \frac{\partial u_j}{\partial x_i} - \frac{2}{3}\delta_{ij}\frac{\partial u_l}{\partial x_l}\right)\right] + \frac{\partial}{\partial x_j}\left(-\rho\overline{u_\iota' u_J'}\right) \qquad (2)$$

$$\frac{D\rho k}{Dt} = \tau_{ij}\frac{\partial u_i}{\partial x_j} - \beta^* \rho\omega k + \frac{\partial}{\partial x_j}\left[(\mu + \sigma_k \mu_t)\frac{\partial k}{\partial x_j}\right] \qquad (3)$$

$$\frac{D\rho\omega}{Dt} = \frac{\gamma}{v_t}\tau_{ij}\frac{\partial u_i}{\partial x_j} - \beta\,\rho\omega^2 + \frac{\partial}{\partial x_j}\left[(\mu + \sigma_\omega \mu_t)\frac{\partial \omega}{\partial x_j}\right] + 2(1 - F_1)\frac{\rho\sigma_{\omega 2}}{\omega}\frac{\partial k}{\partial x_j}\frac{\partial \omega}{\partial x_j} \qquad (4)$$

No-slip boundary conditions were applied to the walls of the root canal and the needle. The root canal walls, and the major apical foramen were considered as a rigid, smooth and impermeable wall. Uniform inlet velocity was applied in accordance with the inlet Reynolds number to needle inlet. Atmospheric pressure as outlet boundary condition was defined at the outlet of the root canal orifice. To realistically reflect the

details of the root canal surface, tetrahedral elements were used for mesh generation. To avoid low quality elements, element sizing for different regions such as needle, apical region and side canals were defined separately. A representative mesh is shown in Figure 3.
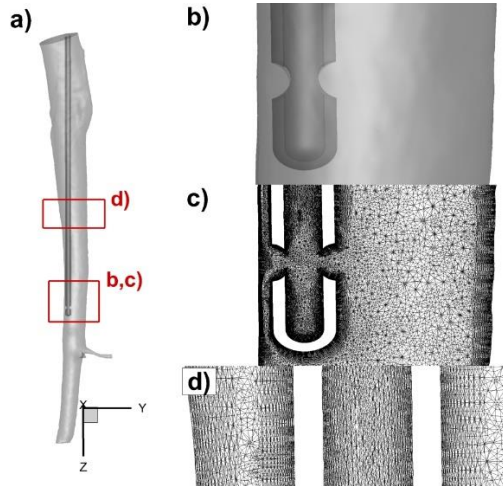

Figure 3. Representative mesh: a) General view, b) Needle tip geometry, c) Mesh near the tip of the needle, d) Mesh of the root canal.

To satisfy the requirements of the turbulence model and precisely predict the development of the hydrodynamic boundary layer, regions adjacent to the walls were purposely refined with inflation layers, thus maximum wall y+ for each mesh was allowed to be less than 3. Effects of the element size and discretization on the numerical solution was investigated with 8 different mesh resolutions. To demonstrate this, apical pressure was assigned as an indicator for mesh independence tests. Results of the mesh independence tests are shown in Figure 4.
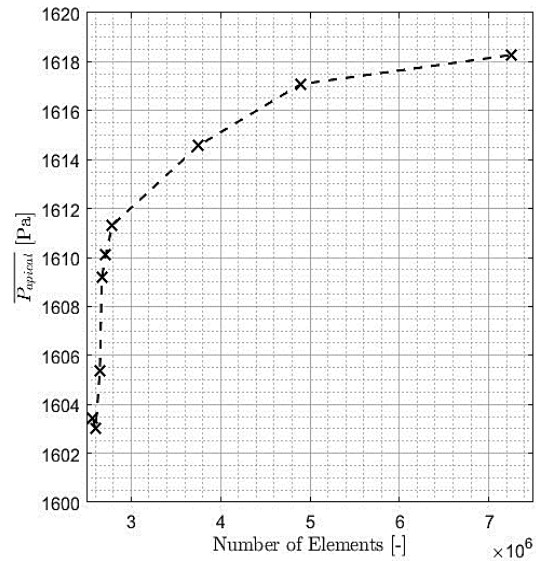

Figure 4. Results of the mesh independence tests. (Model C, Re=1500 and H=1.5 mm)

As can be seen from Figure 4, apical pressure converged to 1618 Pa with increasing number of elements, indicating that a mesh consisting of nearly 4.9 million of elements was sufficient for CFD calculations due to the relative error being less than 0.1%. These calculations were performed on a computer with a 3.7 GHz 8-core 64-bit AMD Ryzen 7 2700X processor, 32 GB RAM and Windows 10 100 Pro operating system.

3. Results

Various cases have been simulated and the velocity maps, pressure distribution of the irrigant and the wall shear stresses in the root canal were compared. In Figure 5, Figure 6 and Figure 7, pressure distribution, velocity magnitude and wall shear are shown for Model A Model B and Model C, respectively.
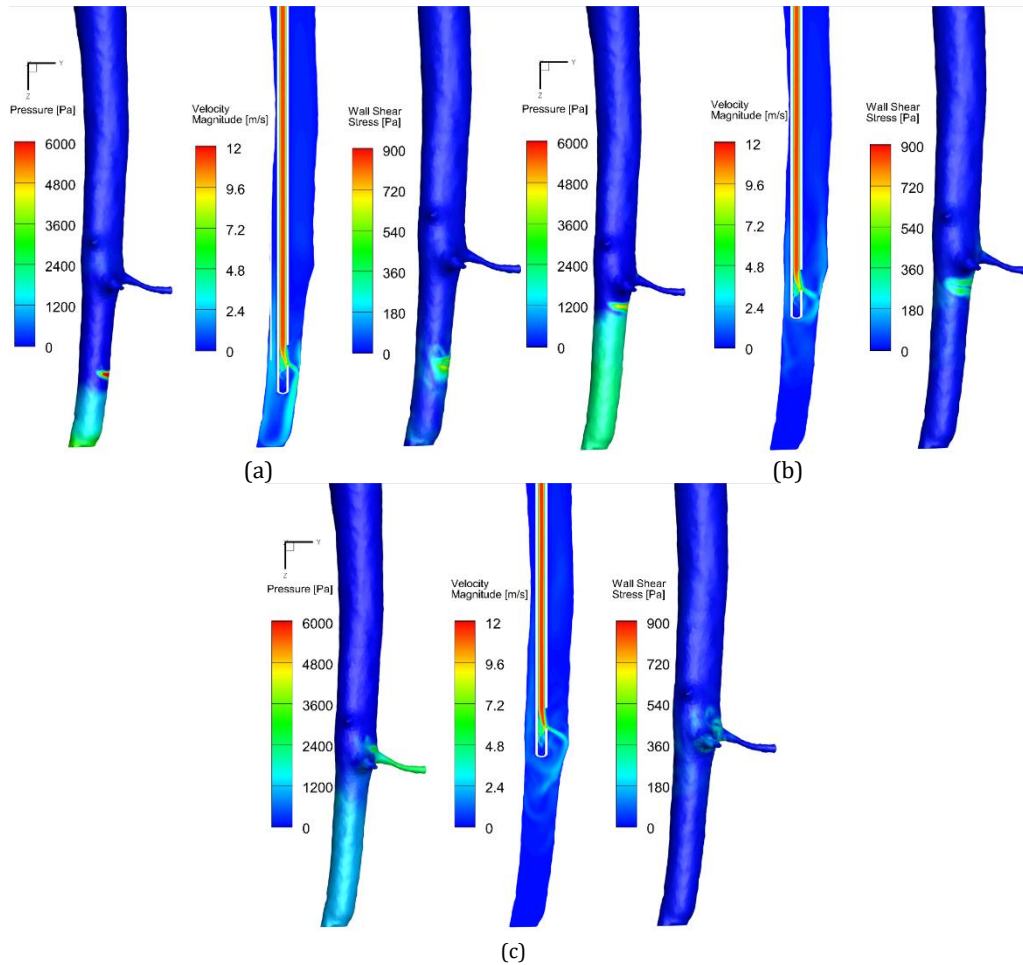
Figure 5. Pressure, velocity, and wall shear stress distributions inside the root canal (with Model A needle) observed for different distances from the working lengths: a) 0.5 mm, b) 1.5mm and c) 3mm.

As can be seen from Figure 5.a, there is a stagnation region where the irrigant flow from the needle exit impinges to the root canal wall. Following that, a wall jet flow occurs in the vicinity of the stagnation and results in a high wall-shear stress region as can be seen in Figure 5.b and Figure 5.c. With increasing distances from the working length (H); pressure in the vicinity of the apical foramen decreases and the position of the stagnation zone changes in accordance. It should be noted that the intensity and characteristics (in terms of pressure and wall shear stress distributions) of the stagnation zone only vary with the topology of the root canal. As can be seen from the velocity distributions shown in Figure 6, due to the momentum effects inside the needle, there is no significant amount of irrigant flow coming out of the top vent exit of the double-side-vented Model B. Resulting stagnation pressure is 22% lower than Model A. With varying working lengths, the effect of the flow at the region of the top vent exit varies in correlation with closeness to the root canal wall. For both Model A and B, the jet flow separates at the needle vent exit. For more performant needles, the effect of vent angle might be considered. Apart from the flow in the vicinity of the top vent exit of Model B, flow characteristics that occurred with Model A and Model B are found to be similar.
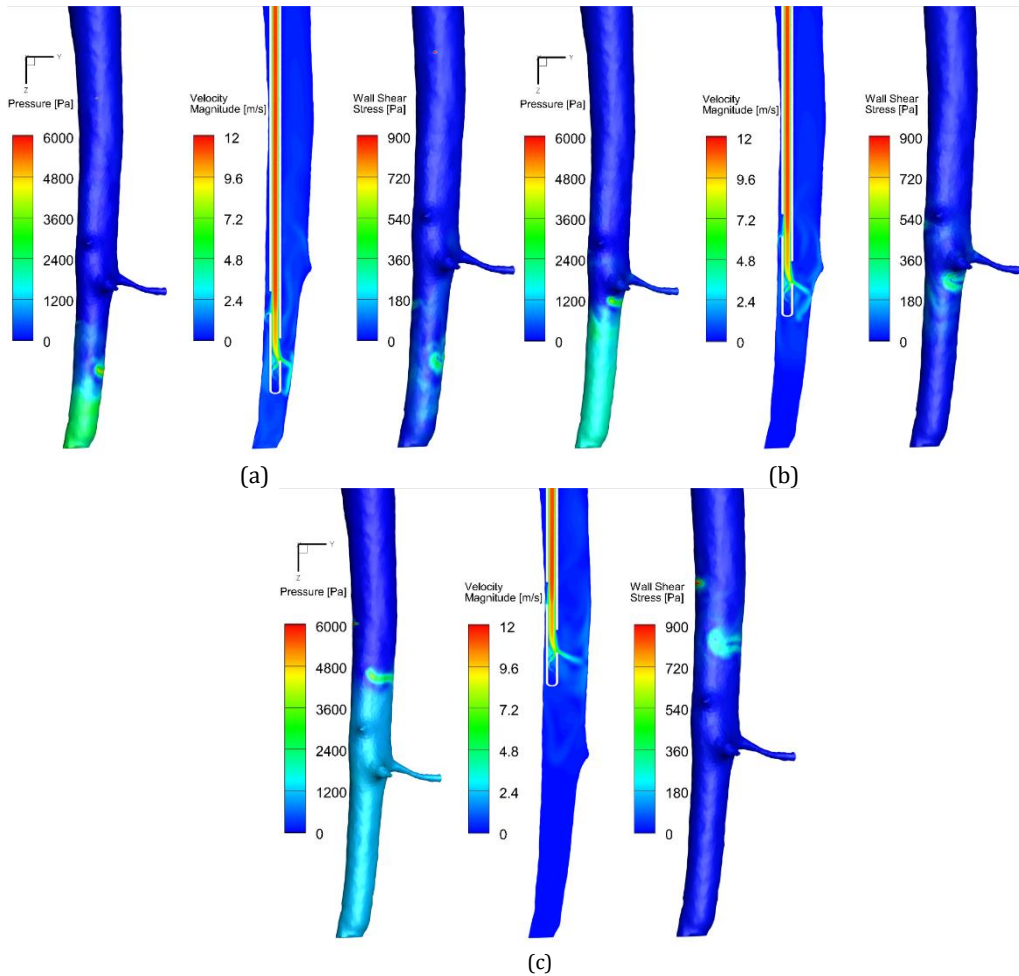
(a)

(b)

(c)

Figure 6. Pressure, velocity, and wall shear stress distributions inside the root canal (with Model B needle) observed for different distances from the working lengths: a) 0.5 mm, b) 1.5mm and c) 3mm.

The main flow pattern was consistent for all simulations. An irrigant jet forms from the bottom opening of the needle directed to the root canal wall. Following the impingement occurring at the root canal wall, the irrigant jet is directed to the apex region while dissipating. The main flow pattern was not affected by the needle opening geometry. It should be noted that all jets became more effective if the flow rates were increased. The most potential jets were formed at the outlet most proximal to the tip, while the flow from the distal outlet presented only a minor influence on the flow structure (Figure 6). Model A and Model B showed a jet flow from the side vent, however Model C created two symmetric jets toward the apical as it has two symmetrical outlets at the same level (Figure 5, Figure 6, and Figure 7). All needles showed similar performances as all of them were closed-ended needles. Model A and model B had asymmetric, Model C had symmetric velocity distributions because of the needle geometry which can be seen in the contours of velocity magnitude (Figure 5, Figure 6 and Figure 7).
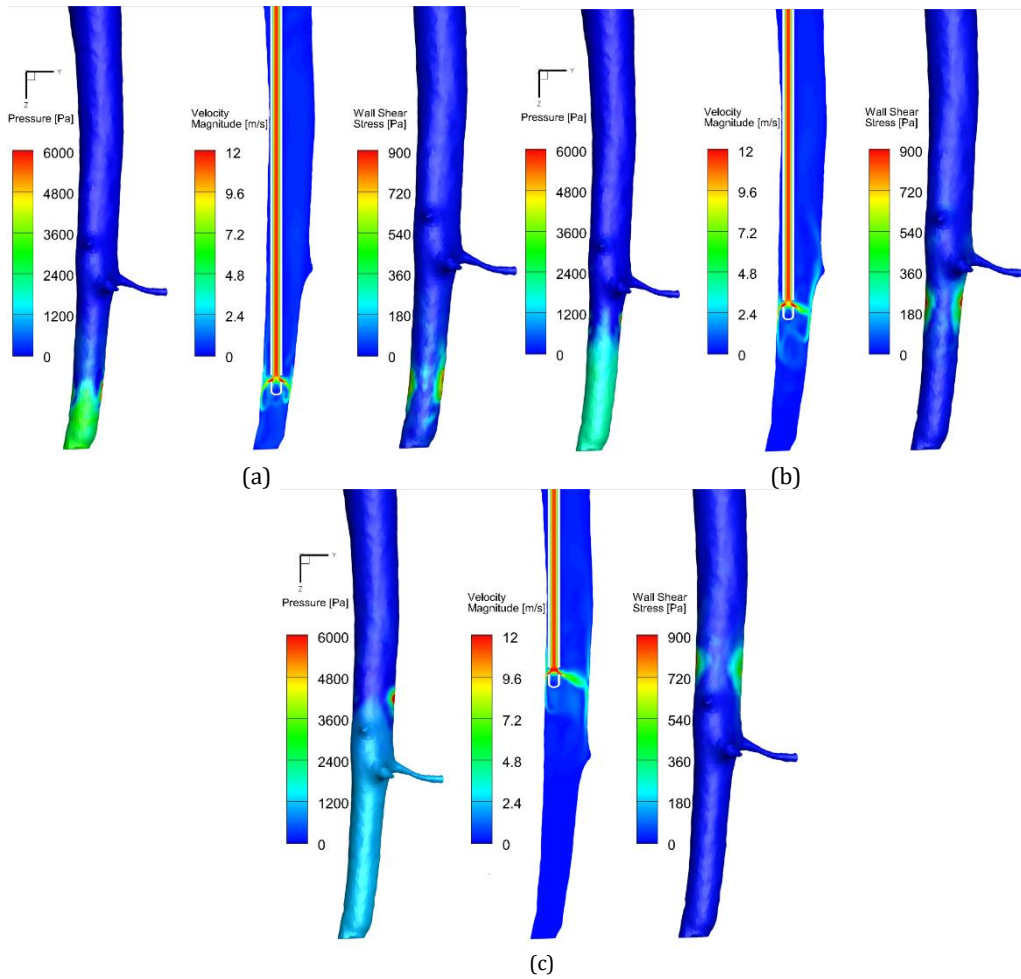
Figure 7. Pressure, velocity, and wall shear stress distributions inside the root canal (with Model C needle) observed for different distances from the working lengths: a) 0.5 mm, b) 1.5mm and c) 3mm.

Approaching the closed-end of the needle, the flow showed sudden deceleration due to the stagnation of the flow. On the other hand, the highest velocities were observed inside the needle lumens for all cases. For all models, depending on insertion depth of the irrigation needle, a stagnation zone was observed in the apical region where the flow could not effectively penetrate. The irrigant coming out of the needle exit, returned towards to the root canal orifice before reaching the apical foramen of the root canal when placed at 1.5 mm or above in the root canal. None of the needle models were able to deliver the irrigant till the working length of H=1.5 mm to 3 mm was selected, as the irrigant

penetration toward the apex was limited. Irrigant could penetrate up to working length of 0.5 mm for all needles.

Figure 8 shows the average wall shear stress distributions on the root canal walls at various Re and H. All models showed similar wall shear-stress distributions and developed the local maxima in the vicinity of their exits (Figure 5, Figure 6 and Figure 7). The maximum wall shear stress was seen in a small area next to the needle outlets. With increasing inlet velocity, the area-weighted wall shear stress also increased for all needle models as shown in Figure 8.

(a)

(b)

(c)

Figure 8. Average wall shear stress distributions with respect to operating conditions (distances from the working length and Re) for different needle models: a) Model A, b) Model B, c) Model C.

The maximum wall shear stress was seen in a small area next to the needle outlets. With increasing inlet velocity, the area-weighted wall shear stress also incre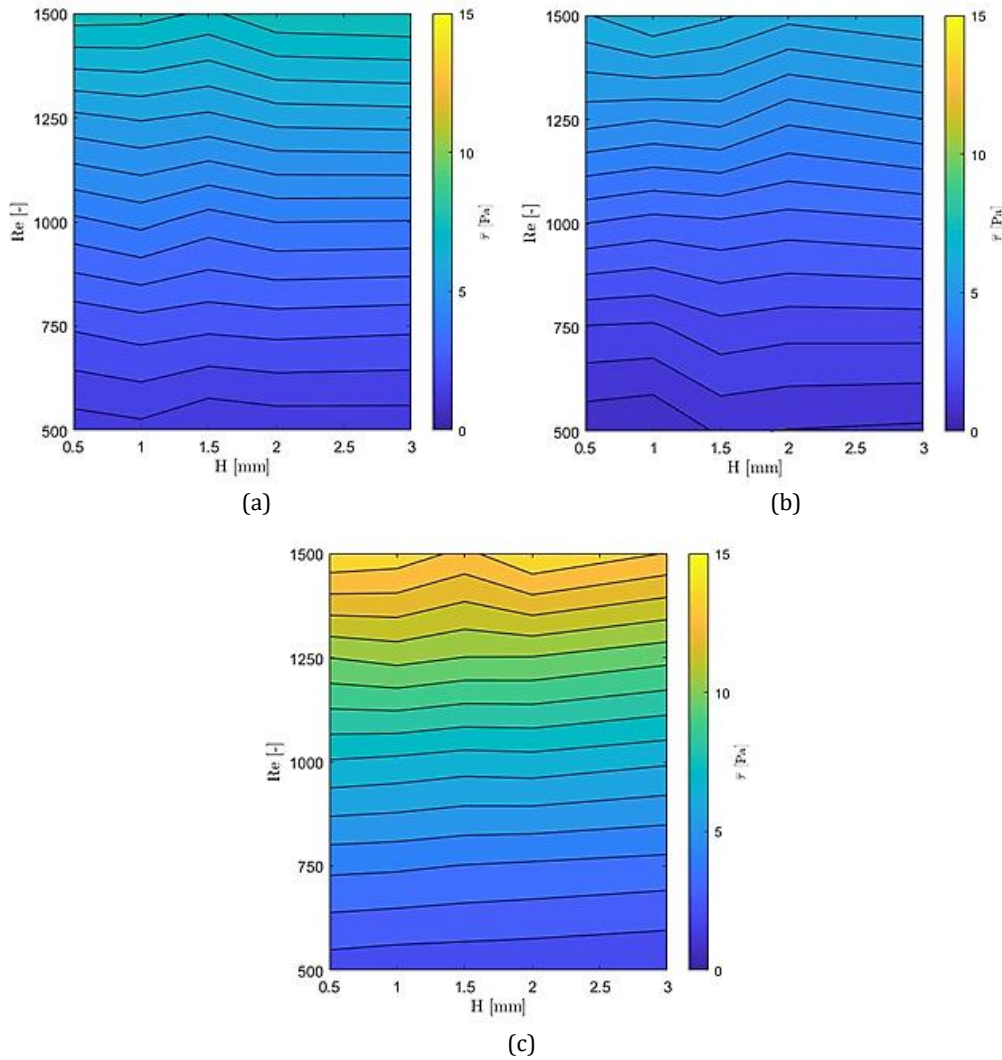ased for all needle models as shown in Figure 8. The wall shear stress was considerably higher for the high Reynolds number cases compared to the low Reynolds number ones, but it was also affected by the needle model. No significant difference was found between the Model A and Model B as they showed identical wall shear stress distributions. Model C revealed the highest wall shear stress among all. It was found out that, when the Re number changes from 500 to 1500, area weighted average wall shear stresses for all models increase by 5.75 ,6.95 and 6.64 times for Model A, Model B and Model C, respectively. It can be concluded that the needle-exit geometry, the needle insertion depth, and the distance of the exit part of the needle from the wall have effects on the pressure distribution of the root canal wall. It was observed that as the working length increased, the distance of the needle-exit to the root canal wall decreased, therefore the pressure on the root canal wall increased for all needle models.
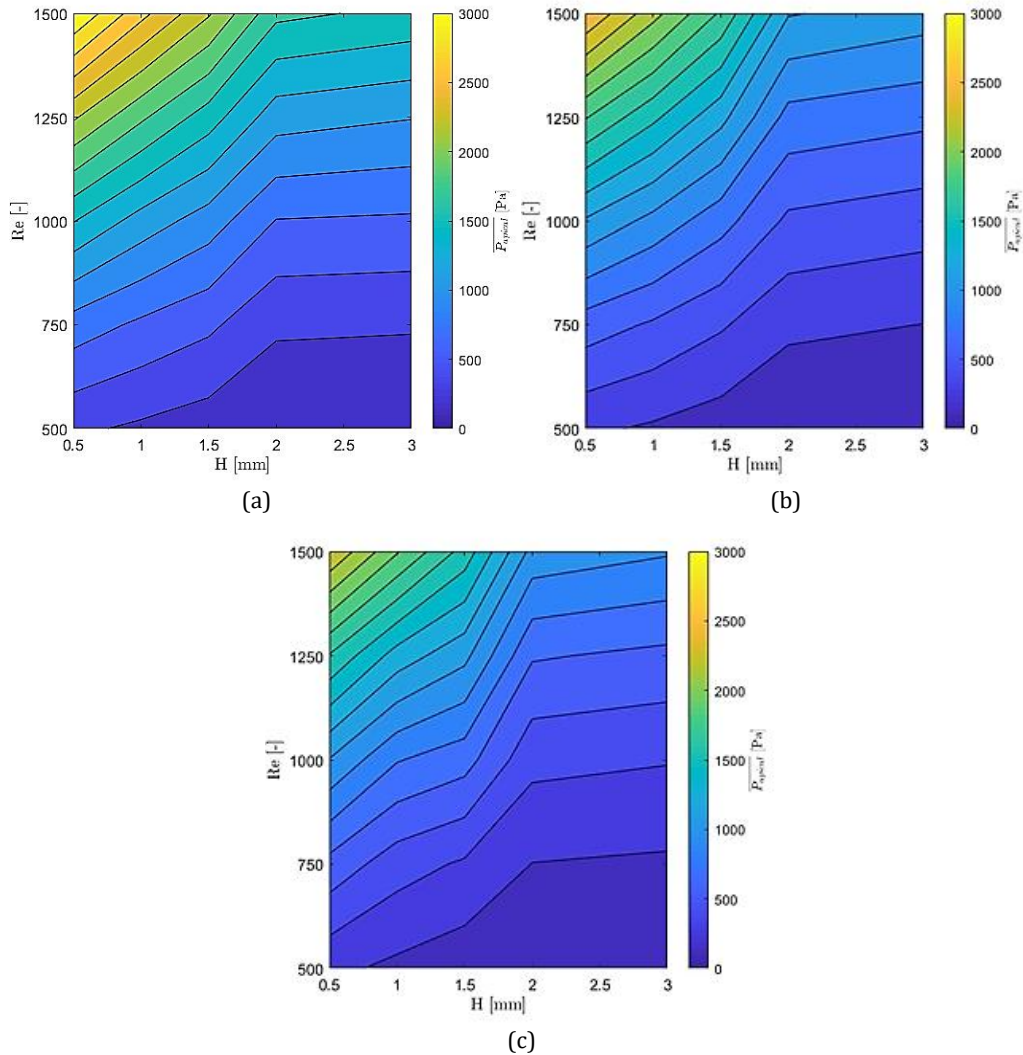
776

(a)

(b)

(c)

Figure 9. Apical Pressure variations with respect to operating conditions (distances from the working length and Re) for different needle models: a) Model A, b) Model B, c) Model C.

In Figure 9, the area-weighted average pressure at the apical foramen for each needle are given and they show that the velocity of the irrigant and the insertion depth of the irrigation needle have significant impact on the apical pressure. Increasing in inlet Re number gradually increased apical pressure. In addition, working length influenced the growth of apical from 0.5 mm to 2 mm needle insertion depth caused to a rapid growth of apical pressure for all needle models. Apical pressure growth was observed to be less progressive at working lengths between 2 mm and 3 mm for all needles. It should be noted that the most rapid growth in apical

pressure was observed between 1.5 mm and 2 mm for all needles. At all Re and needle insertion depths, apical pressures can be given in descending order: Model A, Model B, and Model C. To highlight originality and novelty of the current study, a concise comparison with available studies in the literature and an overall evaluation were made in the next section.

4. Comparison with Literature

This study represents CFD simulations of root canal irrigation using a 3D model of an actual root canal of human maxillary central tooth. The main purpose of this study is to monitor the effect of different irrigation needle geometries

on fluid flow in the root canal and compare the performances of the needles. Three 30-gauge closed-ended irrigation needles were included in this study as it has been reported that small-diameter needles provide more efficient irrigant replacement without forceful apical extrusion [21]. The irrigation needle tips were placed in the apical third of the root canal at a range of 3-6 mm in accordance with other studies ([22], [23]) thus the working length of the needles were selected as 0.5 mm, 1 mm, 1.5 mm, 2 mm and 3 mm. The root canal was assumed to be filled with the irrigant in all cases since possibility of air bubble entrapment was very limited and could be neglected ([24], [25]). Selected inlet Reynolds numbers were within the range applied by clinicians when 30-gauge needles are used [26]. Velocities above 0.1 m/s were considered clinically significant for adequate irrigant replacement [23]. The highest velocity values were at the centreline of the needle lumen, satisfying no-slip boundary conditions on the interior walls of the needle. The flow rate associated with Re has a significant effect on irrigant replacement throughout the root canal, but it does not directly affect flow pattern [17]. Irrigant penetration and wall shear stress on the root canal wall have a significant role in the mechanical cleaning effect and the chemical effect of irrigation ([23], [27], [28]). Models showed a sudden deceleration of the irrigant approaching the needle exit, since the tip of the needle is closed. Stagnant behaviour of the irrigant has been observed in all cases within the apical part of the root canal until the needle was placed under 0.5 mm close to the working length. It is very likely that the apical third of the root canals cannot be sufficiently cleaned and disinfected by syringe irrigation until the irrigation needle is placed very close to the working length. Irrigant replacement was highest for Model C, followed by the Model A and Model B. These results were compatible with earlier studies that also reported limited irrigant exchange ([2], [22], [27]). In Model B that has two needle exits at different levels, irrigant flow rates were not equal between two needle exits and most of the irrigant left through the needle close to the tip of the needle, which is in accordance with previous studies [23]. The wall-shear stress has an impact on the detachment of debris, unfortunately cannot guarantee removal of debris from the root canal wall, unless there is a favourable irrigant flow to carry debris outside of the root canal [23]. Maximum wall shear stress

was observed on the canal wall facing the exit quite close to the tip of the needle (Figure 5, Figure 6 and Figure 7). Increasing the Reynolds number led to a large increase in the wall shear stress in all cases (Figure 8) and it is noteworthy that this significantly affected debris removal from the lateral canals during syringe irrigation. The wall-shear stress distributions on the interior walls of the root canal were similar for the Model A and Model B and it was the highest for Model C, which has the smallest side vent. For Model B, the proximal outlet mostly affected the overall performance, which agreed with previous studies ([23], [29]). A drawback of all needle types was the increase of wall shear stress in a very limited area. When the exit of the irrigation needle was positioned at the same level of the lateral canal in the root canal, there was an increase in the wall shear stress at the entrance of the lateral canal. It can be assumed that the Model C, which produced the highest wall shear stress (Figure 8), was superior to other models in effective irrigation of lateral canals and other irregularities in the root canal. The irrigant jet impinges the closed-ended tip of the needle during irrigation, causing considerably high stagnation pressures within the needle lumen tip. In general, for all needle models, increasing the inlet velocity resulted in higher apical pressures as shown in Figure 9. Irrigant extrusion towards the periapical was associated with forceful delivery of the irrigant and the apical pressure ([23], [27] and [28]). Simulating the apical foramen as an impermeable and rigid wall did not exclude the possibility of irrigant extrusion toward the periapical tissue. The evaluation of irrigant pressure applied at impermeable wall can give information about the possibility of irrigant extrusion [30]. Extrusion of irrigant occurs when the tissue back pressure is overcome by irrigant pressure and the presence of periapical lesions increases the risk ([12], [13] and [21]). It is strongly recommended that needles do not penetrate the walls, as the needle binding to the canal wall will likely result in the blockage of backflow and forced extrusion of the irrigant. It should be noted that, without a validated pressure threshold for irrigant extrusion accidents, it is not possible to determine in which of these cases an accident may occur. Snjaric et al. [32] mentioned that interstitial tissue pressure, ranges from 2666 to 3999 Pa (20-30 mmHg), mean value 3333 Pa (25 mmHg) and pathological conditions can reduce interstitial

tissue pressure to 1333 Pa (10 mmHg), therefore mean interstitial tissue pressure may represent the threshold at which periapical extruding is possible ([13], [31] and [32]). However, apical pressure did not reach 3333 Pa in any analysis performed in the current study. Also, Zhu et al. [33] suggested that when the apical foramen of the tooth is not closed and the apical pressure in the root canal exceeds 30 mmHg (close to intraosseous blood pressure value), NaOCl can extrude through apical foramen. In three analyzes apical pressure was found over 25 mmHg which were Model A with Re=1500 for 0.5 mm and 1 mm and Model B with Re=1500 for 0.5 mm. Model C did not exceed the threshold value under any conditions in all analyzes. Lower apical wall pressure indicates improved safety and reduced risk of apical extrusion. Model C appeared to be safer than other models in terms of apical extrusion (Figure 9). On the contrary, the limited irrigant penetration and the irrigant replacement to the apically necessitates needle placement very close to the apex in the root canal. Especially, Model C can be suggested as the safest among all the models since it satisfies apical extrusion condition at all operating conditions.

5. Conclusion

In the current study micro-computed tomography (micro-CT) analysis was used to numerical model of a maxillary central tooth for a comprehensive and clinically realistic evaluation of the root canal irrigation. Within the limits of the methodology used in present study, it may be concluded that all closed ended side-vented needles are safe for root canal irrigation by new users. The needle tip design influences important parameters for the effectiveness and safety of the root canal irrigation. In all CFD simulations, the risk of extrusion of irrigant was low and the Model C was the most effective and safest design to reduce irrigant extrusion among all.

6. Ethics committee approval and conflict of interest statement

The use of extracted tooth was approved by the Istanbul University Faculty of Dentistry Clinical Research Ethics Committee (2019/31). "The prepared article does not have a conflict of interest with any person / institution."

References.

[1] Loroño, G., Zaldívar, J. M. R., Jimenez-Octavio, J. R., Dorado, S., Arias, A., & Cisneros, R. 2020. CFD analysis on the effect of combining positive and negative pressure during the irrigation of artificial isthmuses. International Journal for Numerical Methods in Biomedical Engineering, 36(10), e3385. DOI: 10.1002/cnm.3385

[2] Zehnder, M. (2006). Root canal irrigants. Journal of endodontics, 32(5), 389-398. DOI: 10.1016/j.joen.2005.09.014

[3] Verma, P., & Love, R. M. (2011). A Micro CT study of the mesiobuccal root canal morphology of the maxillary first molar tooth. International endodontic journal, 44(3), 210-217. DOI: 10.1111/j.1365-2591.2010.01800.x

[4] Villas-Bôas, M. H., Bernardineli, N., Cavenago, B. C., Marciano, M., del Carpio-Perochena, A., De Moraes, I. G.,Ordinola-Zapata, R. 2011. Micro–computed tomography study of the internal anatomy of mesial root canals of mandibular molars. Journal of endodontics, 37(12), 1682-1686. DOI: 10.1016/j.joen.2011.08.001

[5] Lam, M. S., Chang, J. W., & Cheung, G. S. 2021. Ex vivo shaping ability of reciprocating instruments operated by new users: Reciproc versus WaveOne. Clinical Oral Investigations, 25(5), 2791-2799. DOI: 10.1007/s00784-020-03593-x

[6] Esentürk, G., Akkas, E., Cubukcu, E., Nagas, E., Uyanik, O., & Cehreli, Z. C. 2020. A micro-computed tomographic assessment of root canal preparation with conventional and different rotary files in primary teeth and young permanent teeth. International Journal of Paediatric Dentistry, 30(2), 202-208. DOI: 10.1111/ipd.12587

[7] Peters, O. A., Laib, A., Göhring, T. N., & Barbakow, F. 2001. Changes in root canal geometry after preparation assessed by high-resolution computed tomography. Journal of endodontics, Cilt. 27(1), s. 1-6.

[8] Peters, O. A., Laib, A., Göhring, T. N., & Barbakow, F. 2001. Changes in root canal geometry after preparation assessed by high-resolution computed tomography. Journal of endodontics, 27(1), 1-6. DOI: 10.1097/00004770-200101000-00001

[9] Boutsioukis, C., Verhaagen, B., Versluis, M., Kastrinakis, E., & Van Der Sluis, L. W. M. 2010. Irrigant flow in the root canal: experimental validation of an unsteady Computational Fluid Dynamics model using high-speed imaging. International Endodontic Journal, 43(5), 393-403. DOI: 10.1111/j.1365-2591.2010.01692.x

[10] Goldman, M., Kronman, J. H., Goldman, L. B., Clausen, H., & Grady, J. 1976. New method of irrigation during endodontic treatment. Journal of endodontics, 2(9), 257-260. DOI: 10.1016/S0099-2399(76)80085-4

[11] Kahn, F. H., Rosenberg, P. A., & Gliksberg, J. 1995. An in vitro evaluation of the irrigating characteristics of ultrasonic and subsonic handpieces and irrigating needles and probes. Journal of endodontics, 21(5), 277-280. DOI: 10.1016/S0099-2399(06)80998-2

[12] Ram, Salzgeber, R. M., & Brilliant, J. D. 1977. An in vivo evaluation of the penetration of an irrigating

solution in root canals. Journal of endodontics, 3(10), 394-398.
DOI: 10.1016/S0099-2399(77)80172-6

[13] Z. 1977. Effectiveness of root canal irrigation. Oral Surgery, Oral Medicine, Oral Pathology, 44(2), 306-312.
DOI: 10.1016/0030-4220(77)90285-7

[14] Abou-Rass, M., & Piccinino, M. V. 1982. The effectiveness of four clinical irrigation methods on the removal of root canal debris. Oral Surgery, Oral Medicine, Oral Pathology, 54(3), 323-328.
DOI: 10.1016/0030-4220(82)90103-7

[15] Sedgley, C., Applegate, B., Nagel, A., & Hall, D. (2004). Real-time imaging and quantification of bioluminescent bacteria in root canals in vitro. Journal of endodontics, 30(12), 893-898.
DOI: 10.1097/01.DON.0000132299.02265.6C

[16] Raj, S., Dhingra, A., Jha, P., Nikhil, V., Ravinder, R., & Mishra, P. 2021. To compare the continuous and intermittent irrigation method on the removal of dentin debris from root canals and to evaluate the dynamics of irrigant flow using computational fluid dynamics. Journal of Conservative Dentistry: JCD, 24(1), 94-99.
DOI: 10.4103/jcd.jcd_636_20

[17] Perry, R.H., Green, D. W., & Southard, M. Z. 2019. Perry's chemical engineers' handbook. McGraw-Hill Education.

[18] Boutsioukis, C., Lambrianidis, T., Verhaagen, B., Versluis, M., Kastrinakis, E., Wesselink, P. R., & van der Sluis, L. W. 2010. The effect of needle-insertion depth on the irrigant flow in the root canal: evaluation using an unsteady computational fluid dynamics model. Journal of Endodontics, 36(10), 1664-1668.
DOI: 10.1016/j.joen.2010.06.023

[19] Ansys, I. 2011. ANSYS FLUENT theory guide. Canonsburg, Pa, 794.

[20] Menter, F. R. 1992. Improved two-equation k-omega turbulence models for aerodynamic flows (No. A-92183).

[21] Druttman, A. C. S., & Stock, C. J. R. 1989. An in vitro comparison of ultrasonic and conventional methods of irrigant replacement. International Endodontic Journal, 22(4), 174-178.
DOI: 10.1111/j.1365-2591.1989.tb00920.x

[22] Boutsioukis, C., Lambrianidis, T., & Kastrinakis, E. 2009. Irrigant flow within a prepared root canal using various flow rates: a computational fluid dynamics study. International Endodontic Journal, Cilt. 42(2), s. 144-155.
DOI: 10.1111/j.1365-2591.2008.01503.x

[23] Boutsioukis, C., Verhaagen, B., Versluis, M., Kastrinakis, E., Wesselink, P. R., & van der Sluis, L. W. 2010. Evaluation of irrigant flow in the root canal using different needle types by an unsteady computational fluid dynamics model. Journal of endodontics, 36(5), 875-879.
DOI: 10.1016/j.joen.2009.12.026

[24] Guerisoli, D. M. Z., Silva, R. S. D., & Pécora, J. D. 1998. Evaluation of some physico-chemical properties of different concentrations of sodium hypochlorite solutions. Braz Endod J, 3(2), 21-3.

[25] Gulabivala, K., Ng, Y. L., Gilbertson, M., & Eames, I. 2010. The fluid mechanics of root canal irrigation. Physiological measurement, 31(12), 49.

[26] Boutsioukis, C., Lambrianidis, T., Kastrinakis, E., & Bekiaroglou, P. 2007. Measurement of pressure and flow rates during irrigation of a root canal ex vivo with three endodontic needles. International Endodontic Journal, 40(7), 504-513.
DOI: 10.1111/j.1365-2591.2007.01244.x

[27] Shen, Y., Gao, Y., Qian, W., Ruse, N. D., Zhou, X., Wu, H., & Haapasalo, M. 2010. Three-dimensional numeric simulation of root canal irrigant flow with different irrigation needles. Journal of Endodontics, 36(5), 884-889.
DOI: 10.1016/j.joen.2009.12.010

[28] Wang, R., Shen, Y., Ma, J., Huang, D., Zhou, X., Gao, Y., & Haapasalo, M. 2015. Evaluation of the effect of needle position on irrigant flow in the C-shaped root canal using a computational fluid dynamics model. Journal of endodontics, 41(6), 931-936.
DOI: 10.1016/j.joen.2015.02.002

[29] Vinothkumar, T. S., Kavitha, S., Lakshminarayanan, L., Gomathi, N. S., & Kumar, V. 2007. Influence of irrigating needle-tip designs in removing bacteria inoculated into instrumented root canals measured using single-tube luminometer. Journal of endodontics, 33(6), 746-748.
DOI: 10.1016/j.joen.2007.02.013

[30] Lambrianidis, T., Tosounidou, E., & Tzoanopoulou, M. 2001. The effect of maintaining apical patency on periapical extrusion. Journal of Endodontics, 27(11), 696-698.
DOI: 10.1097/00004770-200111000-00011

[31] Guyton, A. C., Granger, H. J., & Taylor, A. E. 1971. Interstitial fluid pressure. Physiological reviews, 51(3), 527-563.
DOI: 10.1152/physrev.1971.51.3.527

[32] Šnjarić, D., Čarija, Z., Braut, A., Halaji, A., Kovačević, M., & Kuiš, D. 2012. Irrigation of human prepared root canal–ex vivo based computational fluid dynamics analysis. Croatian medical journal, 53(5), 470-479.
DOI: 10.3325/cmj.2012.53.470

[33] Zhu, W. C., Gyamfi, J., Niu, L. N., Schoeffel, G. J., Liu, S. Y., Santarcangelo, F., ... & Tay, F. R. (2013). Anatomy of sodium hypochlorite accidents involving facial ecchymosis—a review. Journal of dentistry, 41(11), 935-948.
DOI: 10.1016/j.jdent.2013.08.012